American Mineralogist, Volume 68, pages 426–443, 1983

The high-frequency vibrational spectra of vitreous and crystalline orthosilicates

BERNARD PIRIOU

ER 60210 Elements de transition dans les solides
C.N.R.S. Bellevue, 1 Place Aristide Briand,
92190 Meudon, France

AND PAUL MCMILLAN

Department of Chemistry
Arizona State University
Tempe, Arizona 85287

Abstract

The Raman spectrum of vitreous $CaMgSiO_4$ is described in detail, and compared with that of polycrystalline monticellite, and the Raman spectra of polycrystalline forsterite, merwinite and β- and γ-Ca_2SiO_4 are presented. The relevant literature is reviewed to identify a consistent set of high-frequency vibrational modes for the olivines, and the assignment of these modes to ν_1- and ν_3-derived vibrations of the orthosilicate units is discussed. The role of vibrational mode coupling within the high-frequency band set is considered, and a simple coupling model is proposed which shows reasonable agreement with the observed spectra. Finally, tetrahedral bond lengths and angles from a number of structural refinements are examined, and some systematics are discussed in relation to the observed high-frequency spectra.

Introduction

The olivines and related crystalline orthosilicates are of considerable importance to igneous and metamorphic petrology, and have been the subject of extensive structural studies. We have prepared polycrystalline samples of calcium magnesium orthosilicates in a solar furnace, and report their Raman spectra. We previously reported the preparation of $CaMgSiO_4$ glass (McMillan *et al.*, 1981), whose Raman spectra showed an intense polarized band at 854 cm^{-1}, assigned to the symmetric stretching vibration (ν_1) of tetrahedral orthosilicate units.

The glass spectrum was compared with that of polycrystalline monticellite ($CaMgSiO_4$ olivine), which showed two intense bands at 852 and 817 cm^{-1}. These two crystal modes are derived from symmetric ν_1 and asymmetric ν_3 stretching vibrations of the SiO_4 tetrahedra (see *e.g.*, Herzberg, 1945; Servoin and Piriou, 1973). From the comparison of $CaMgSiO_4$ crystal and glass spectra, it appears that the 852 cm^{-1} crystal mode should be assigned to the ν_1-derived vibration. The olivines forsterite (Mg_2SiO_4), tephroite (Mn_2SiO_4) and γ-Ca_2SiO_4, and the orthosilicate larnite (β-Ca_2SiO_4), also have two intense Raman modes in the 800–850 cm^{-1} region. Most previous studies have assigned the lower-frequency band to the ν_1-derived vibration, in contrast to the present assignment from the $CaMgSiO_4$ glass and crystal comparison. This apparent conflict led to an examination of the vibrational spectroscopic literature on olivines, where we found a number of inconsistencies, both in observed Raman and infrared spectra and in band assignments. In the section on assignment of high-frequency modes we consider the results of the present study along with the relevant literature to identify a consistent set of high-frequency infrared and Raman bands for silicate olivines, and discuss their assignment to vibrational modes.

The isotopic exchange experiments of Pâques-Ledent and Tarte (1973) and the results of vibrational calculations suggested that ν_1- and ν_3-derived vibrations in the olivines might be strongly coupled. This is discussed in the section on vibrational mode coupling, where a simple coupling model is presented for Raman-active high-frequency modes, in reasonable agreement with the observed frequency shifts and relative intensity changes.

Finally, a number of studies have attempted to relate systematic changes in olivine high-frequency vibrations to compositional parameters. We have examined a number of olivine structure refinements in a search for systematics which may be correlated with the vibrational spectra. Variations in tetrahedral bond lengths and angles for olivines and related orthosilicate are considered in the section on orthosilicate crystal structures, while the relationship of these variations to the high-frequency vibrational spectra is discussed in the final section.

0003–004X/83/0304–0426$02.00

Experimental

Sample preparation

The $CaMgSiO_4$ sample was prepared from a gel, while all others were prepared from reagent-grade oxide mixes. Details of pre-fusion heating may be found in Table 1, along with analyses after melting. The samples were melted in a 2.5 kW vertical axis solar furnace at C.N.R.S. Odeillo, France. Crystalline samples were prepared by removal of the sample from the beam and allowing to cool in air. Samples for "super quench" were subjected to an initial fusion to compact the sample, then fusion followed by splat quenching onto a cooled metal surface. The quench rate by this method is estimated at 10^5–10^6°C s^{-1}. Further details of the method are given by Coutures *et al.* (1978). Temperature at the sample could not be controlled or measured, and substantial temperature gradients must have existed. All samples were observed to melt, giving liquid globules, and glass was found in fast-quench experiments, hence it was assumed that temperatures attained were in excess of the sample melting points. Glass formation was verified by X-ray and optical examination, using a polarizing microscope.

Crystalline samples of β- and γ-Ca_2SiO_4, merwinite and forsterite were analyzed by electron microprobe; $CaMgSiO_4$ crystal and glass by X-ray fluorescence, and a sample of vitreous $CaMgSiO_4$ by energy-dispersive scanning electron microscopy. The results of these analyses are given in Table 1, along with experimental details of each analytical technique. Evaporation of component oxides is known to occur in solar furnace experiments, and previous work in the system CaO–MgO–SiO_2 (McMillan, 1981, and ms. submitted) has shown that the rate of component loss increases in the order CaO < SiO_2 < MgO. This is consistent with the observed sample compositions in Table 1. The Ca_2SiO_4 samples completely crystallized to

Table 1. Sample preparation and analysis details

	β-Ca_2SiO_4	γ-Ca_2SiO_4	$Ca_3Mg(SiO_4)_2$
	(b)	(b)	(b)
CaO (a)	67.5 ± 0.7	67.2 ± 0.6	51.5 ± 2.4
MgO	--	--	14.8 ± 3.2
SiO_2	32.5 ± 0.7	32.8 ± 0.6	33.7 ± 3.6

	$CaMgSiO_4$ (crystal)	$CaMgSiO_4$ (glass)		Mg_2SiO_4	
	(c)	(c)	(d)	(b)(e)	(b)(f)
CaO	33.4 ± 0.5	33.2 ± 0.5	33.7	--	--
MgO	32.9 ± 0.5	32.4 ± 0.5	31.8	67.0 ± 1.4	48.1 ± 8.3
SiO_2	33.8 ± 0.5	34.3 ± 0.5	34.5	33.0 ± 1.5	51.9 ± 8.3

Oxide mixes were ground 15-30 mins. under acetone, dried 4-6 hours at 200°C, heated 6-8 hours at 1000°C. Gel mix was heated 48 hours at 1300°C, then 20 hours at 1400°C. Both were solar melted and cooled normally for polycrystalline samples. The $CaMgSiO_4$ glass was fused a second time followed by "super-quench".

Notes:

(a) Mole% oxide, normalied to 100%. Only the Mg_2SiO_4 crystalline sample gave poor weight % oxide sums (near 95%), presumably due to poor carbon coating at glass/crystal interfaces (e.g. Coons, 1978). All other weight % oxides summed to 98 - 102%.
(b) Electron microprobe analyses using a Cameca MS46, with 15 kV voltage and 20nA beam current. Standards were natural diopside, wollastonite, enstatite and forsterite, and data reduced with Heinrich's (1972) program FRAME. Errors are two standard deviations of around twenty points for each sample.
(c) X-ray fluorescence analyses using the low-dilution disc method of Thomas and Haukka (1978) with a Philips PW 1410 vacuum spectrometer. Errors are estimated.
(d) Analysis by energy-dispersive scanning electron microscopy (Aden and Buseck, 1979).
(e) crystalline parts of sample.
(f) coexisting inhomogeneous glass.

Table 2. Observed Raman bands for Ca, Mg orthosilicates and tephroite

Forsterite Mg_2SiO_4					Monticellite $CaMgSiO_4$			Tephroite Mn_2SiO_4		
(a)	(b)	(c)	(d)		(d)	(c)		(d)	(e)	
825.5	826	824.3	822	A_g	817	817.5	A_g	804	808	A_g
839	839	837	835	B_{1g}					820	B_{1g}
856	856	856.4	854	A_g	849	851.7	A_g	838	839	A_g
866	866	866	863	B_{1g}						
881	884	881	880	B_{2g}		884(1)				
920	922	919	917	B_{3g}	899	900 ~920(1)	B_{3g}	891	892	B_{3g}
966	966	965	960	A_g	947	949.5	A_g	932	935	A_g
975.5	976	975	972	B_{1g}						

γ-Ca_2SiO_4			Larnite β-Ca_2SiO_4				Merwinite $Ca_3Mg(SiO_4)_2$
(h)	(c)		(g)	(f)	(c)		(c)
			818(2)				
818	813.6	A_g	848	841	846.8	A_g	845(3)
							860(3)
							872
840	839.4	A_g	860	860	860.7	A_g	887
	849	B_{1g}?		882	876	B_g?	911
							921
			900	900	899	A_g	939
				917	916.5	B_g?	980
888	887	B_{3g}					991
			979	979	978	A_g?	1011
926	925	A_g					

Notes: All frequencies are in cm^{-1}. (1) Due to merwinite: see text. (2) Probably due to traces of γ-Ca_2SiO_4. (3) Perhaps due to traces of β-Ca_2SiO_4.

References to Table 2: (a) Servoin and Piriou (1978); (b) Iishi (1978); (c) This study; (d) Hohler and Funck (1973); (e) Stidham et al. (1976); (f) Conjeaud and Boyer (1980); (g) Hanke and Ptaak (1978); (h) Spectrum taken by Mrs. H. Boyer; appears in applications publicity, entitled "Calcium silicates" and "Application to certain cements", for MOLE microprobe, Jobin-Yvon Instruments S.A., 16 Rue du Canal, 91160 Longjumeau, France.

silica-deficient calcium orthosilicates, while the Mg_2SiO_4 sample gave stoichiometric forsterite in a silica-rich glass matrix. The $CaMgSiO_4$ sample showed minor composition change, perhaps due to its preparation from a gel mix. Before any analytical work, the samples were examined by optical microscopy. The Mg_2SiO_4 sample was observed to contain a small amount (5–10%) of glass; all others were entirely crystalline. X-ray powder patterns were run on a Philips Norelco diffractometer from 5–60° 2θ, using Cu$K\alpha$ radiation. All orthosilicate patterns corresponded with the latest literature values. The X-ray pattern of Mg_2SiO_4 showed a broad, weak hump at low 2θ, probably due to the amorphous phase, while the monticellite sample was found to contain some merwinite. This is in agreement with phase equilibrium studies in the system Mg_2SiO_4–Ca_2SiO_4 (Biggar and O'Hara, 1969; Warner and Luth, 1973), which showed that monticellite is never stoichiometric $CaMgSiO_4$ at 1 atm, but is Ca-

Table 3. Source references for Figure 5(a–c)

Olivines			
(1)	Brown (1980), Table A4, p. 362-364: from Brown (1970; Ph.D. thesis).		
	Ni	Ni_2SiO_4	synthetic
	Co	Ca_2SiO_4	synthetic
	Kn	$(Fe_{.51}Mn_{.46}Mg_{.02})_2SiO_4$	knebellite
	*Gl	$(Ca_{.49}Mn_{.46}Mg_{.05}Fe_{.004})_2SiO_4$	glaucochroite
	*Ki	$(Ca_{.57}Fe_{.43})_2SiO_4$	kirschsteinite
	Zn-Pi	$(Mn_{.65}Mg_{.17}Zn_{.11}Fe_{.06})_2SiO_4$	zincpicrotephroite
(2)	Lager and Meagher (1978)		
	Ni	Ni_2SiO_4	synthetic
	Mo	$(Ca_{.5}Mg_{.465}Fe_{.035})_2SiO_4$	monticellite
	Gl	$(Ca_{.49}Mn_{.435}Mg_{.05}Zn_{.025})_2SiO_4$	glaucochroite
(3)	Brown (1980): re-refined from Birle et al. (1968)		
	Fo	$(Mg_{.90}Fe_{.10})_2$	forsterite
	Ho	$(Mg_{.49}Fe_{.49}Mn_{.01}Ca_{.01})_2SiO_4$	hortonolite
	Fa	$(Fe_{.92}Mg_{.04}Mn_{.04}Ca_{.002})_2SiO_4$	fayalite
(4)	Hazen (1976)		
	*Fo	Mg_2SiO_4	synthetic forsterite
(5)	Francis and Ribbe (1980)		
	Pi	$(Mi_{.514}Mn_{.482}Ca_{.003}Fe_{.001})_2SiO_4$	picrotephroite (Fo_{51})
	Te	$(Mn_{.890}Mg_{.091}Ca_{.0065}Fe_{.013})_2SiO_4$	tephroite (Te_{91})
(6)	Brown (1980): re-refined from Onken (1965)		
	Mo	$(Mg_{.5}Ca_{.5})_2SiO_4$	monticellite
(7)	Hazen (1977)		
	*Fa	Fe_2SiO_4	synthetic fayalite
(8)	Czaya (1971)		
	Ca	Ca_2SiO_4	synthetic γ-Ca_2SiO_4
(9)	Ghose and Wan (1974)		
		$Co_{1.10}Mg_{0.90}SiO_4$	synthetic
(10)	recalculated from Smyth and Hazen (1973)		
	Fo	Mg_2SiO_4	synthetic forsterite
	Mo	$Mg_{0.75}Fe_{1.10}Mn_{0.15}SiO_4$	hortonolite
(11)	Brown and Prewitt (1973). (O-O distances calculated)		
	Mo	$Mg_{1.64}Fe_{0.35}Ca_{0.01}(Si_{0.99}Al_{0.01})O_4$	lunar (12052)
	Mo	$Mg_{1.42}Fe_{0.58}(Si_{0.99}Al_{0.01})O_4$	lunar (12018)
	Mo	$Mg_{1.38}Fe_{0.60}Ca_{0.01}Cr_{0.01}(Si_{0.99}Al_{0.01})O_4$	(OG2B)

deficient. Our near-$CaMgSiO_4$ stoichiometry had then crystallized monticellite plus merwinite.

After "super-quenching," the major part of the $CaMgSiO_4$ sample was crystalline: only the thinnest edges and fibers were entirely vitreous. Attempts to polish samples for Raman spectroscopy were unsuccessful due to the small size (often less than 0.5 mm) and extremely delicate nature of suitable fragments. Glass samples were selected by trial and error for those giving the most intense Raman spectrum with minimum scattering of the incident laser beam, and maximum retention of its polarization.

The excitation source for Raman spectroscopy was the 5145 or 4880Å line of a Spectra-Physics 165 Ar^+ laser, with scattering geometry of 90° into a Coderg PHO double monochromator. The spectra of polycrystalline samples were obtained by near-90° scattering with the incident beam at a glancing angle to the excited surface. All crystal spectra were run with resolving slits of 2 cm^{-1}, while 6 cm^{-1} slits were used for the glass spectra. Finally, the spectrum of merwinite was obtained with a Coderg triple monochromator in the Laboratoire d'Optique Appliquée, ENSTA, Palaiseau, using similar conditions to those described above.

Experimental results

The high-frequency (>800 cm^{-1}) lattice modes of the olivines may be described in terms of coupled stretching vibrations of the four SiO_4 tetrahedra in the unit cell. The expected high-frequency Raman-active modes may be obtained by factor-group analysis (*e.g.*, Fateley *et al.*, 1972). Eight bands are expected, two derived from the symmetric ν_1 vibration of the isolated tetrahedron, and six from its asymmetric stretch ν_3. One ν_1-derived mode

Table 3. (continued)

(12)	Smyth (1975). (O-O distances calculated)		
	*Fa	Fe_2SiO_4	synthetic
(13)	Rajamani et al. (1975). (O-O; O-Si-O calculated)		
		$Ni_{1.03}Mg_{0.97}SiO_4$	synthetic
(14)	Morimoto et al. (1974)		
	*	Co_2SiO_4	synthetic
(15)	Basso et al. (1975). Ten natural (Mg,Fe) olivines.		
	3G9	$Fo_{91.5}$	3G19 Fo_{91}
	3G12	$Fo_{90.5}$	3G51 Fo_{91}
	3G15	$Fo_{90.5}$	2488 $Fo_{93.5}$
	3G17	$Fo_{89.5}$	2500 Fo_{91}
	3G18	$Fo_{92.5}$	2501 Fo_{91}
(16)	Wenk and Raymond (1973). Four natural (Mg,Fe) olivines.		
		$(Mg_{0.95}Fe_{0.012}Mn_{0.003})_2SiO_4$	Yosemite 103-481
		$(Mg_{0.893}Fe_{0.099}Ni_{0.008})_2SiO_6$	Bergell Alps Sci 59
		$(Mg_{0.672}Fe_{0.319}Ni_{0.004}Ca_{0.005})_2SiO_4$	Apollo 12
		$(Mg_{0.637}Fe_{0.358}Ca_{0.005})_2SiO_4$	Apollo 11
(17)	Finger (1970). Two natural (Mg,Fe) olivines.		
		$(Mg_{1.463}Fe_{0.529}Ca_{0.008})_2SiO_4$	10020
		$(Mg_{0.98}Fe_{1.013}Ca_{0.007})_2SiO_4$	C15-16
(18)	Hanke (1965)		
	Fo	$(Mg_{0.9}Fe_{0.1})_2SiO_4$	natural forsterite
	Fa	Fe_2SiO_4	natural fayalite
Non-olivines			
(19)	Cruickshank (1964): re-refined from Midgley (1952)		
	*La	Ca_2SiO_4	synthetic β-Ca_2SiO_4
(20)	Yamaguchi and Suzuki (1967) (distances and angles calculated)		
	Mw	$Ca_3Mg(SiO_4)_2$	synthetic merwinite
(21)	Moore and Araki (1972). (O-Si-O calculated)		
	Mw	$Ca_3Mg(SiO_4)_2$	synthetic merwinite

Note; *denotes refinements not used for Figure 5, as discussed in text.

is of A_g symmetry, as are two ν_3-derived vibrations. Correlated with these three A_g modes by the unit cell symmetry (Davydov splitting) are three B_{1g} modes, one from ν_1, and two from ν_3. The two remaining ν_3-derived modes have B_{2g} and B_{3g} symmetry (see Table 4, and Servoin and Piriou, 1973).

The observed crystal spectra are displayed in Figures 1 and 2; the left side of the figure showing the complete spectra to near 1000 cm^{-1}, while on the right appear details of the high frequency region. It may be seen that the frequency range covered by the high-frequency modes, due mainly to the site-group splitting of ν_3-derived vibrations, is around 100 cm^{-1}, much larger than the Davydov splitting (A_g–B_{1g}) which is never more than 15 cm^{-1}. The site-group splitting appears generally to decrease in the order forsterite (Fo) > monticellite (Mo) > γ-dicalcium silicate (γ-C_2S), while the relative intensities of the two strongest modes change continuously in the same sequence. These observations form the basis for much of the discussion in the present report.

Figure 1a shows the Raman spectrum of polycrystalline forsterite, Mg_2SiO_4. The vibrational mode symmetries have been assigned from the single crystal studies of Servoin and Piriou (1973) and Iishi (1978). The B_{3g} and B_{2g} modes at 919 and 881 cm^{-1} are readily attributed to ν_3-derived vibrations, as may be the high-frequency A_g mode at 965 and its related B_{1g} at 975 cm^{-1}. However, the attribution of the A_g modes at 824 and 856 cm^{-1}, and their correlated B_{1g} modes at 837 and 866 cm^{-1}, to ν_1- and ν_3-derived vibrations is not evident.

The Raman spectrum of polycrystalline monticellite appears in Figure 1b. The spectrum is comparable with the single-crystal study of Hohler and Funck (1973), except for the band at 884 and the weaker feature near 920 cm^{-1}. These are due to bands of merwinite which was identified as an impurity from the X-ray pattern. The monticellite band symmetries have been taken from the work of Hohler and Funck. Only the three A_g modes and the single B_{3g} were distinguished in both their study and the present work. The B_{3g} at 900 and A_g at 949 cm^{-1} may

Table 4. Factor group analyses for larnite (β-Ca_2SiO_4) and merwinite ($Ca_3MgSi_2O_8$), and summarized for olivine (M_2TO_4)

Larnite β-Ca_2SiO_4: Midgley (1952); Cruikshank (1964). Monoclinic space group $P2_{1/n}$ (C_{2h}^5); z = 4 (28 atoms). All atoms in general positions 4(e) of symmetry C_1. Total modes: Γ^M = 21 A_g + 21 A_u + 21 B_g + 21 B_u. Infrared active: 20 A_u + 19 B_u; Raman active: 21 A_g + 21 B_g.

Site analysis at $\underline{k} = \underline{0}$:

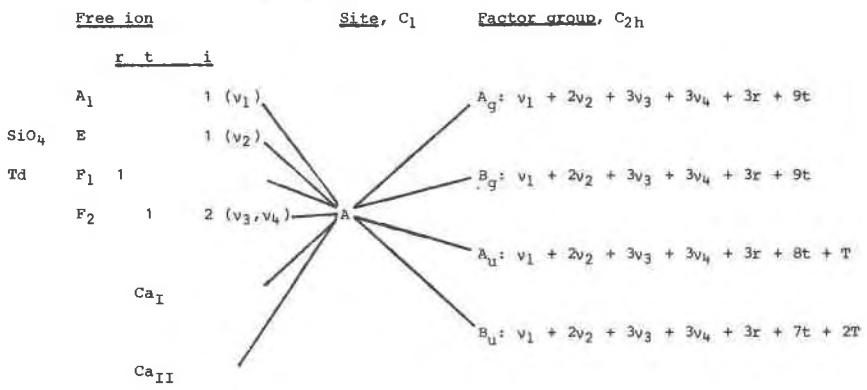

(T denotes acoustic mode)

Raman active high-frequency internal modes:

$$\nu_1 \longrightarrow A_g + B_g$$

Merwinite $Ca_3Mg(SiO_4)_2$: Yamaguchi and Suzuki (1967); Moore and Araki (1972): monoclinic space group $P2_{1/a} = C_{2h}^5$; z = 4 (56 atoms).

point group 2/m = C_{2h}

All atoms in general positions 4(e) of symmetry C_1.

The factor group analysis is identical to that for larnite with twice as many vibrational degrees of freedom.

Total vibrations: Γ^M = 42 A_g + 42 A_u + 42 B_g + 42 B_u

Infrared active: 41 A_u + 40 B_u; Raman active: 42 A_g + 42 B_g

Raman active high-frequency internal modes of SiO_4

$$\nu_1 \longrightarrow 2A_g + 2B_g$$

$$\nu_3 \longrightarrow 6A_g + 6B_g$$

Olivine structure M_2TO_4: see Table 3, and Servoin and Piriou (1973) for factor group analysis.

Orthorhombic space group Pbnm (C_{2h}^{16}), z = 4.

Total modes: Γ^M = 11 A_g + 7 B_{1g} + 11 B_{2g} + 7 B_{3g} + 10 A_u + 10 B_{2u} + 14 B_{3u}

Raman active high-frequency internal modes:

$$\nu_1 \longrightarrow A_g + B_{1g} + B_{2g} + B_{3g}$$

$$\nu_3 \longrightarrow 2A_g + 2B_{1g}$$

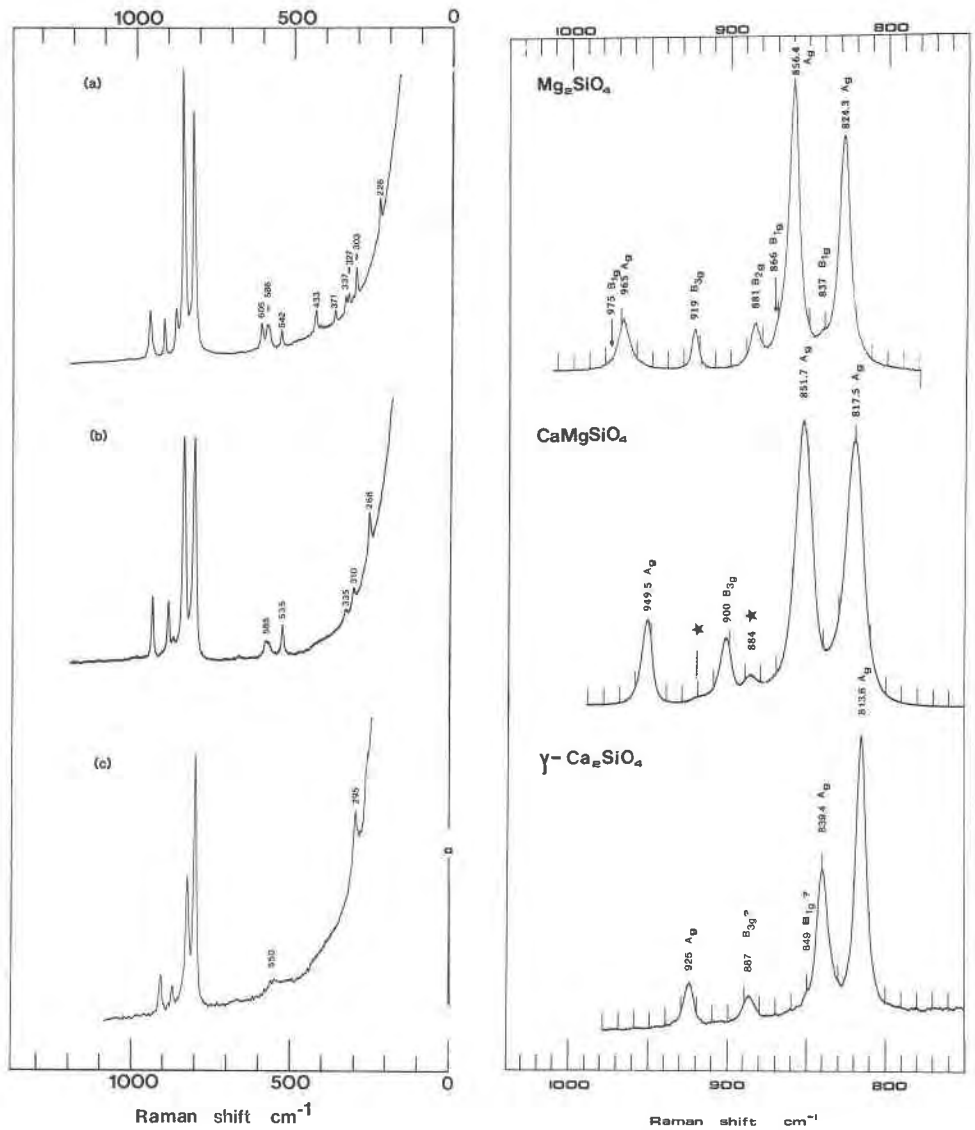

Fig. 1. Raman spectra of polycrystalline (a) forsterite, (b) monticellite and (c) γ-Ca_2SiO_4. Overall spectra on left, and detail of high-frequency bands on right. Bands marked (*); see Table 2 and text.

be attributed to ν_3-derived vibrations. However, as for forsterite, the A_g bands at 852 and 817 may not easily be assigned.

Figure 1c shows the Raman spectrum of γ-Ca_2SiO_4, which compares well with one obtained by H. Boyer in the Jobin-Yvon Applications Laboratory (see notes to Table 2 for full reference). Its spectrum may be partly assigned by comparison with those of forsterite and monticellite. The bands at 925 and 887 cm^{-1} are probably A_g and B_{3g} modes derived from ν_3, while the weak shoulder at 849 cm^{-1} may be a B_{1g} mode related to the A_g band at 839 cm^{-1}, or could be the expected B_{2g} mode. Once more, the problem arises of assigning the strong A_g modes at 839 and 814 cm^{-1} to ν_1- and ν_3-derived vibrations. Finally, we note a similar assignment problem in the spectrum of tephroite, (Mn_2SiO_4), which has two intense A_g bands at 839 and 808 cm^{-1} (Stidham *et al.*, 1976).

Figure 2 presents the Raman spectra of larnite and merwinite. That of β-Ca_2SiO_4 is similar to spectra obtained by Conjeaud and Boyer (1980), and by Handke and Ptaak (1978). Larnite has a monoclinic unit cell based on the K_2SO_4 structure (Midgley, 1952; Cruickshank, 1964; Eysel and Hahn, 1970), while merwinite is also monoclinic, and related to the larnite structure (Yamaguchi and Suzuki, 1967; Moore and Araki, 1972). A factor group analysis for β-Ca_2SiO_4 is shown in Table 4. Eight high-frequency, Raman-active internal modes are expected;

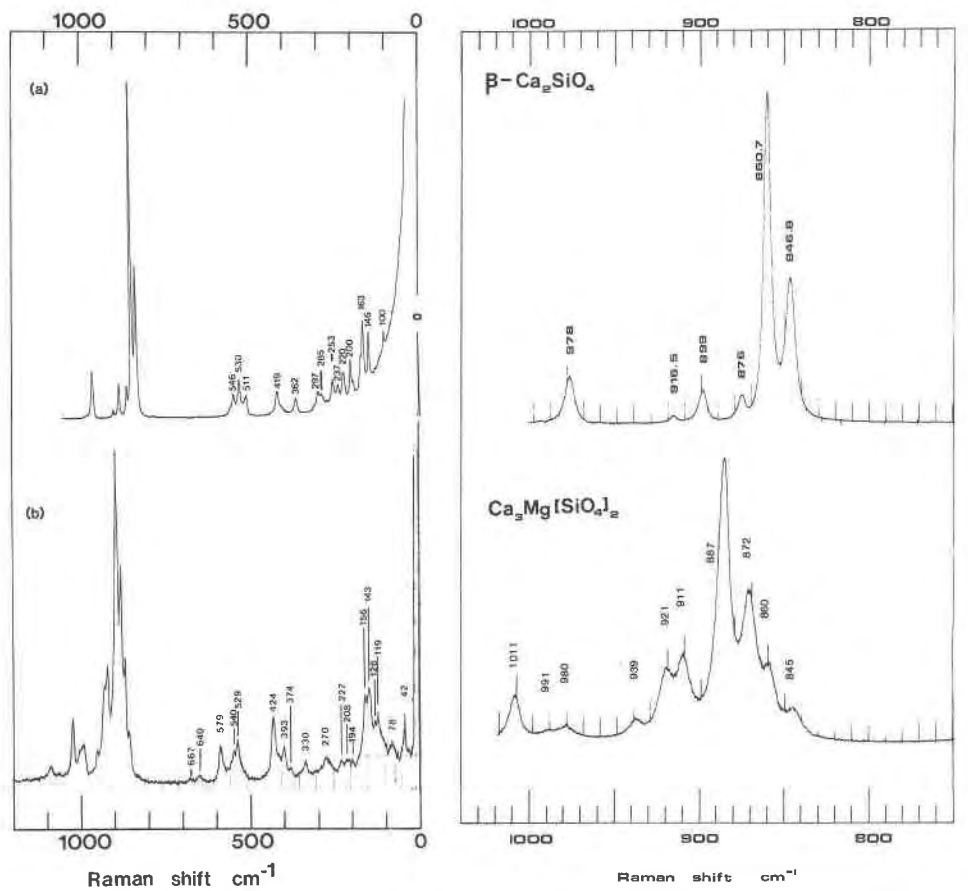

Fig. 2. Raman spectra of polycrystalline (a) larnite and (b) merwinite. Overall spectra on left, and detail of high-frequency bands on right.

four of A_g symmetry and four B_g modes, each correlated with an A_g mode by the Davydov splitting. One A_g, B_g pair is derived from the ν_1 vibration, and the three remaining pairs from ν_3. No assignment of band symmetries may be made from the single crystal study of Handke and Ptaak (1978), and their band at 818 cm^{-1} does not appear in our spectrum and is probably due to some γ-Ca_2SiO_4 phase as impurity. On the basis of relative intensities, we have tentatively assigned the bands of β-Ca_2SiO_4 at 978, 899, 861 and 847 cm^{-1} to A_g modes. The weaker bands at 917 and 876 have then been assigned to B_g modes correlated with the A_g modes at 899 and 861 cm^{-1} respectively. This gives a Davydov splitting of 16 cm^{-1}, comparable with that found for the olivines above, and supporting this assignment. The A_g band at 978 and the A_g, B_g pair at 899 and 917 may be attributed to ν_3-derived vibrations. However, as in the olivines, the assignment of the A_g, B_g pair at 861 and 876 and the A_g at 847 to the remaining ν_3- and ν_1-derived vibrations is not evident. The factor group analysis for merwinite is also described in Table 4, and is identical to that for larnite, but with the number of vibrational modes doubled. The three bands at 860, 845 and 980 cm^{-1} in the merwinite spectrum could be due to a trace of β-Ca_2SiO_4 impurity. No attempt has been made to assign band symmetries, although the strong bands at 887 and 872 cm^{-1} are probably A_g modes.

The polarized spectrum of vitreous $CaMgSiO_4$ (McMillan *et al.*, 1981) is reproduced in Figure 3, compared with the spectrum of polycrystalline monticellite. Due to the nature of the glass sample, which prevented polishing of plane faces for Raman study, the two polarizations may not be pure, and some mixing of VV and VH spectra may be present. Assignment of the observed bands is discussed in the next section.

Discussion

The spectrum of $CaMgSiO_4$ glass

The spectrum consists of an intense, highly-polarized band at 854 cm^{-1}, with a very broad, depolarized, high-frequency shoulder of medium intensity (Figs. 3, 4). A weak, polarized band occurs at 704 cm^{-1}, and a weak doublet with maxima near 580 and 530 cm^{-1}, of which the

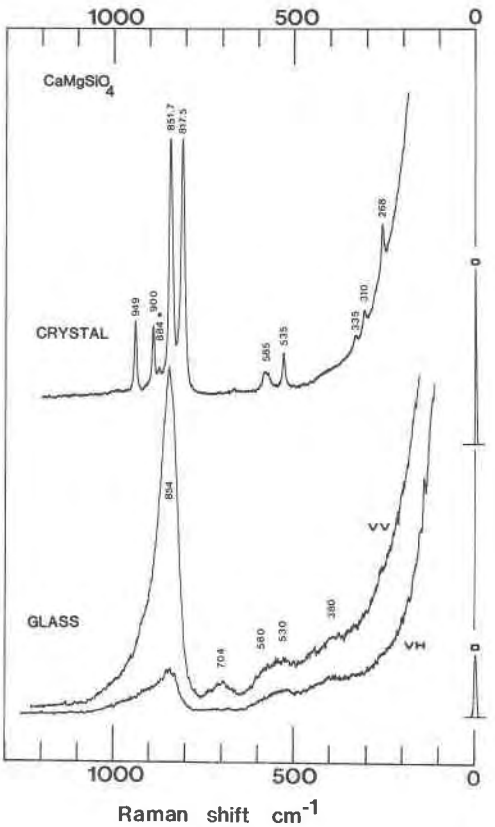

Fig. 3. Raman spectrum of polycrystalline monticellite (top) and polarized spectra of vitreous $CaMgSiO_4$ (bottom).

higher-frequency component is more polarized (Fig. 3) (McMillan *et al.*, 1981).

Infrared spectra of orthosilicate crystals (*e.g.*, Tarte, 1963); Servoin and Piriou, 1973) suggest that bands derived from the ν_3 vibration occur between 850 and 1000 cm^{-1}, while weak sharp peaks in the 800–850 cm^{-1} region have been attributed to ν^{-1}. Raman spectra of aqueous silicate solutions (Fortnum and Edwards, 1956) showed a band near 777 cm^{-1}, which was assigned to ν_1 of hydrated SiO_4 groups. (A band at 935 cm^{-1} was observed, which was associated with the SiO_4 vibrations. It is tempting to assign this to the ν_3 vibration, but our unpublished preliminary data on aqueous silicate solutions suggest that this region is complicated by vibrations of higher silicate polymers.) Considering all these data we expected a strong Raman band in the 800–850 cm^{-1} region for the symmetric ν_1 vibration of isolated SiO_4 tetrahedra in our $CaMgSiO_4$ glass. This band has A_1 symmetry, and should be completely polarized. A broadened, depolarized band was expected at higher frequency for components of the ν_3 vibration, of F_2 symmetry. We have assigned the strong, polarized band observed at 854 cm^{-1} to the ν_1 vibration of the isolated SiO_4 unit, and its depolarized, high frequency shoulder mainly to ν_3-type vibrations.

In an orthosilicate glass, the SiO_4 tetrahedra vibrate nearly independently in the absence of translational symmetry. The A_1 band at 854 cm^{-1} in $CaMgSiO_4$ glass is then a ν_1 vibration of an isolated SiO_4 tetrahedron, perturbed by interaction with Ca^{2+} and Mg^{2+}. Crystal modes derived from coupling of ν_1 vibrations within the unit cell might be expected to have a similar frequency to the free ion ν_1 if the tetrahedron were not too distorted and coupling of ν_1 and ν_3 motions were minimal. However, phonons derived from combination of ν_3 motions should have no counterpart in the glass spectrum, being a function of the crystal symmetry.

It may be seen from Figure 3 that the ν_1 band of $CaMgSiO_4$ glass corresponds closely with the A_g mode at 852 cm^{-1} of monticellite. This suggests the assignment of this A_g, and its associated B_{1g} mode (not observed) to ν_1-derived vibrations. This is also suggested by Figure 4, which shows the behavior of the high-frequency bands as $CaMgSiO_4$ glass is crystallized by laser heating. The 854 cm^{-1} band appears common to crystal and glass, while

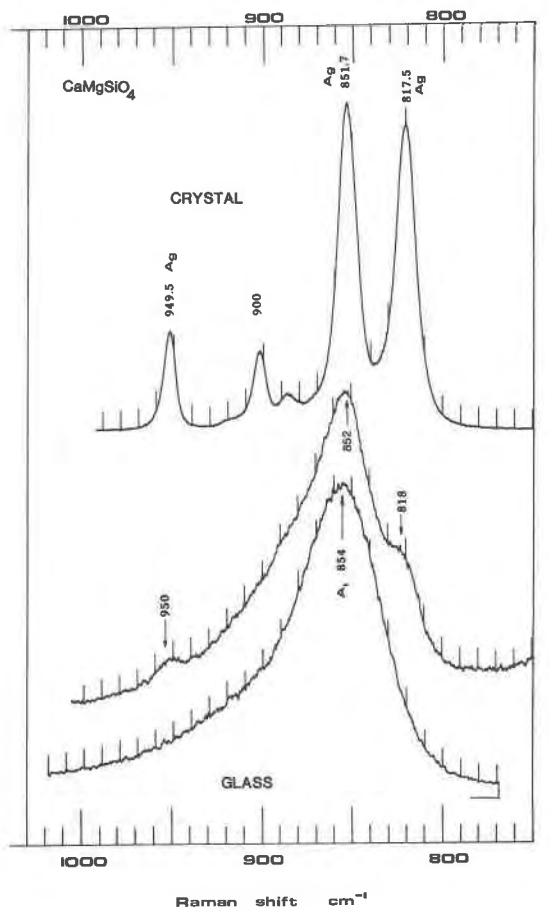

Fig. 4. High-frequency detail of Raman spectrum of polycrystalline monticellite (top) and VV spectrum of $CaMgSiO_4$ (bottom). Sequence bottom to top follows the spectral changes on crystallization of the glass sample by laser heating.

the others appear to grow as crystallization proceeds, suggesting the attribution of the 853 cm^{-1} A_g mode to a ν_1-derived vibration. This is discussed more fully in the following sections.

The weak double band at 520–600 cm^{-1} in the glass may be partly assigned to the asymmetric deformation ν_4 of the SiO_4 tetrahedron, by comparison with the crystal spectrum. The weak, polarized band at 704 cm^{-1} has no counterpart in the crystal spectrum. No bands are expected in this region for modes of SiO_4 units, and vibrations of Ca–O or Mg–O linkages are expected at much lower frequencies (*e.g.*, Lazarev (1972) p. 174–175; Nelson and Exarhos, 1979). The most probable attribution is to the symmetric stretch of Si–O–Si groups in higher silicate polymer species. A polarized band occurs in the region 700–600 cm^{-1} in crystalline pyrosilicates; its frequency dependent on the Si–O–Si angle and the cation–oxygen bonding (*e.g.* Lazarev (1972) p. 66–69; Bretheau-Raynal *et al.*, 1979). A weak band was observed near 700 cm^{-1} by Mysen *et al.* (1980) and McMillan (1981, and ms. submitted) in glasses of composition near $CaMgSiO_4$, increasing in intensity with increasing silica content. This assignment implies the presence of stretch bands due to higher silicate polymers in the region 900–1000 cm^{-1}. These contributions may exist, but would be masked by the SiO_4 vibrations. Consistent with this, the glass analysis showed the SiO_2 content to be slightly high, due to loss of MgO component by evaporation (Table 1). Finally, the weak depolarized band near 380 cm^{-1} may be partly due to Ca–O vibrations. A similar feature has been observed in other Ca-containing oxide glass systems (*e.g.*, Mysen *et al.*, 1980; McMillan, 1981, and ms. submitted). We suggest that part of the double band at 530 and 580 cm^{-1} might be due to MgO vibrations, but have no confirmation for this.

We are not aware of any other work on calcium or magnesium orthosilicate glasses, but a number of Raman studies have been carried out on basic $CaO–SiO_2$ and $MgO–SiO_2$ glasses (Mysen *et al.*, 1980; Virgo *et al.*, 1980; Kashio *et al.*, 1980; McMillan, 1981, and ms. submitted). All observed a sharp, polarized band at 850–860 cm^{-1} whose intensity decreased rapidly with increasing silica content, and which may be attributed to the ν_1 vibration of isolated SiO_4 tetrahedra in these systems. The frequency of this vibration seems to vary little on substitution of Mg for Ca, which is of interest for the later discussion of variation of band frequencies with composition in crystalline orthosilicates.

Kusabiraki and Shiraishi (1981) have reported the IR powder transmission spectrum of vitreous Fe_2SiO_4. They find a strong, broad band centered near 900 cm^{-1} for ν_3 vibrations of the isolated tetrahedra, consistent with the above discussion of $CaMgSiO_4$ glass. However, these authors assign a weak IR band at 695 cm^{-1} to the ν_1 vibration, which seems unjustified in view of the IR and Raman work on crystalline fayalite, where ν_1 is identified at 832 cm^{-1}. Unlike the Raman spectrum, the non-polar ν_1 mode should not appear in the IR absorption, but if present, would be expected as a weak shoulder in the 820–860 cm^{-1} region. Their 695 cm^{-1} band is probably related to vibrations of more polymerized silicate species. These polymers will also contribute to the high frequency part of the Fe_2SiO_4 glass infra-red spectrum reported by Kusabiraki and Shiraishi.

Orthosilicate crystal structures

Before beginning the discussion of the vibrational spectra of the olivines and related orthosilicates, it is necessary to consider their crystal structures. The olivine structure has been described in detail by Brown (1980). The near-octahedral cation sites are distorted, and are split into two populations; the M(1) and M(2) sites. The tetrahedral sites T are also distorted. Much effort has been devoted to investigating the systematics of and reasons for these distortions. Such studies are far from being conclusive or concluded, and are reviewed by Brown (1980).

One point noted by Brown (p. 314) is that, for all silicate olivines studied, the average tetrahedral Si–O distance is remarkably constant, and that neither this nor individual Si–O distances correlated with octahedral cation size. In the present study, tetrahedral bond lengths and angles from forty olivine refinements were compared (see Table 3 for data sources). As already noted by several authors, (*e.g.*, Birle *et al.*, 1968; Louisnathan and Gibbs, 1972) the longest bond is generally Si–O(2), and the shortest Si–O(1). Some structural analyses quoted in Table 3 deviate from this; Smyth's (1975) and Hazen's (1977) refinements for fayalite, and Brown (1980) (from Brown, 1970) for kirschsteinite. The analysis for kirschsteinite has not been repeated and may be correct, but the fayalite refinements do not agree with those of Birle *et al.* (1968) or Hanke (1965), and have not been considered in this study. Hazen's (1976) analysis for forsterite, and the Co_2SiO_4 analysis of Morimoto *et al.* (1974), are likewise incompatible with the general trends, having a much lower Si–O(2) distance than those of other similar refinements. Finally, Brown's (1970) (see Brown, 1980) refinement for glaucochroite is not consistent with that of Lager and Meagher (1978), nor with the overall trend, and has likewise been ignored. The analysis of Czaya (1971) was used for γ-Ca_2SiO_4.

On examination of the 34 olivine refinements considered, it was observed that not only the average Si–O distance, but the individual tetrahedral lengths and angles were similar, apart from those for γ-Ca_2SiO_4. Since the only difference between γ-Ca_2SiO_4 and the other olivines is the presence of Ca on the M(1) site, the M(1) cation was used as a differentiating parameter. The size of the M(1) site was taken as the average value of M(1)–O distances, and Figure 5 shows plots of tetrahedral Si–O and O–O lengths and O–Si–O angles versus <M(1)–O>. All lines drawn have been fitted to the data by linear regression excluding γ-Ca_2SiO_4. It is emphasized that these plots are

not intended to have a structural significance, but are to allow differentiation of γ-Ca_2SiO_4 from the other olivines by plotting of tetrahedral parameters on a common scale. No attempt was made to separate the trends of the angles and edges involving the apical oxygen O(1): these were each treated as one population with a generally decreasing trend. In γ-Ca_2SiO_4 unlike the other olivines, the lengths Si–O(2) and Si–O(3), the edges O(2) and O(3), and the angles O(2)–Si–O(3) and O(3)–Si–O(3), are all nearly equal. This gives the SiO_4 unit nearly C_{3v} symmetry: much higher than the C_s encountered in the other olivines. This may be partly due to the large size of Ca^{2+} tending to "equalize" the two M sites, and minimizing their differences in polyhedral edge-sharing effects.

Several workers have examined the effects of polyhedral edge sharing on polyhedral distortions in the olivine structure, and on bonding in general (reviewed by Brown (1980), p. 329–334). It appears that a high degree of edge-sharing involves generally longer bonds in the component polyhedra. Merwinite is an orthosilicate with no tetrahedral–octahedral edge-sharing, as opposed to the olivines (Moore and Araki, 1972). Its tetrahedral parameters have been plotted on the right side of Figure 5, on the same scale as the olivines. It may be seen that the merwinite Si–O bond lengths are generally shorter than those of the olivines. The structure of β-Ca_2SiO_4 was determined by Midgley (1952), and re-refined by Cruickshank (1964), but is not good enough for direct comparison with the olivine and merwinite parameters plotted in Figure 5. (In fact, Midgley (1952, p. 312) stated that the oxygen positions were not exactly fixed from the experimental data, and that quoted bond lengths were not particularly significant.) However, from the refinements, and the drawing of Eysel and Hahn (1970), it may be seen that the SiO_4 units in β-Ca_2SiO_4 share only one edge (O(3)–O(4)) with the CaO_6 octahedron. This is much less edge-sharing than in the olivines, and might suggest a shorter average Si–O distance than in γ-Ca_2SiO_4.

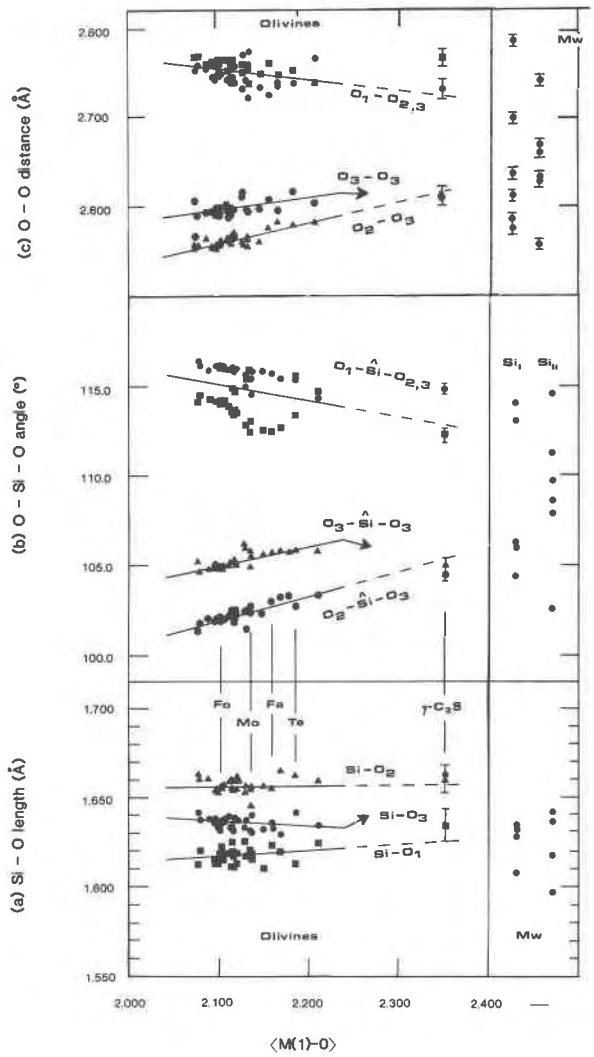

Fig. 5. Variation with ⟨M(1)–O⟩ of olivine tetrahedral distances and angles from refinements in Table 3. For clarity, error bars are not shown for the non-Ca olivines, but are generally quoted as near the size of the plotted points. The merwinite points at right are not plotted *vs.* ⟨M(1)–O⟩, but are shown for comparison with the olivine values. The error bars shown for merwinite and γ-Ca_2SiO_4 are one estimated standard deviation from positional parameters.

Assignment of high frequency modes

Symmetry coordinates. In order to assign the observed bands to specific vibrational modes, it is useful to consider the internal stretching modes of the SiO_4 tetrahedra in terms of symmetry coordinates. When there is no coupling between these internal modes, the symmetry coordinates become identical with the normal coordinates. Figure 6 shows the symmetry coordinates of the modes derived from ν_1 and ν_3 vibrations of SiO_4, similar to those of Oehler and Günthard (1969). For forsterite, the frequency assignment given in this figure will be discussed in the following two sections, and clearly shows the effect of both Davydov and site-group spitting. The ν_1-derived modes at 838 (B_{3u}) and 837.5 (B_{2u}), and the ν_3-derived modes at 877 (B_{3u}) and 983 cm^{-1} (B_{2u}) have net zero dipole moments from this schema, consistent with their observed low oscillator strengths. This also shows that the departure from pure symmetry coordinates is not too great, at least for infrared-active vibrations. This is not the case for the Raman-active modes observed in A_g and B_{1g} symmetries, as discussed below.

The ν_3-derived motions give rise to three families of modes which may be distinguished with respect to the crystallographic axes. The first involves a motion parallel to *a* of silicon against the apical oxygen O(1) (second line in Figure 6). These give rise to the highest frequency modes within each symmetry, consistent with the observation that Si–O(1) is always the shortest distance in the olivine structure. The second type of vibration is predom-

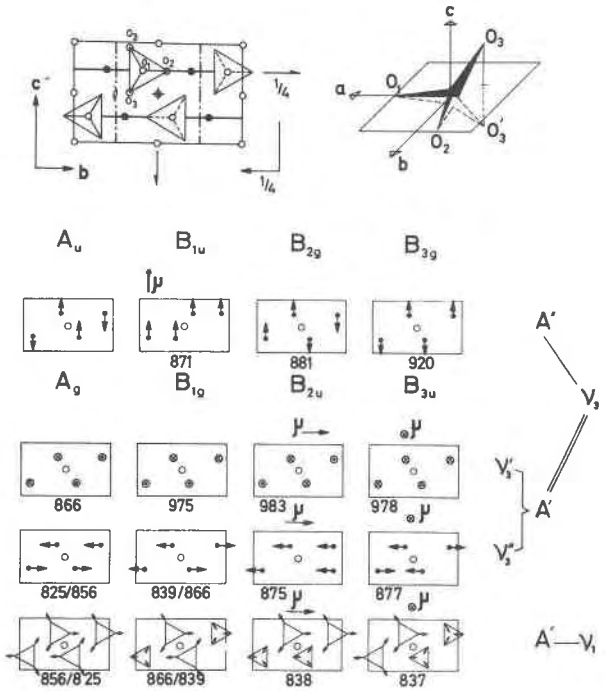

Fig. 6. Symmetry coordinates of high-frequency modes in forsterite. $\vec{\mu}$ is the induced dipole moment. A′ and A″ denote the types of motion relative to the C_s symmetry of SiO_4 groups. Shown above are symmetry elements of the Pbnm space group relative to the unit cell, and the individual SiO_4 units.

inantly a movement of silicon against oxygen O(2) in the *b*-direction (third line in Figure 6). The Si–O(2) distance is the longest tetrahedral bond length in the olivines, and these bands are the lowest frequency ν_3-derived modes. Finally, the motion of silicon in the *c*-direction is mainly against oxygens O(3), with an intermediate Si–O bond length, giving rise to a group of frequencies intermediate between the two families above.

Infra-red results. The bands in the 800–1000 cm^{-1} region of orthosilicate crystal spectra may be attributed to modes derived from ν_1 and ν_3 internal vibrations of the SiO_4 tetrahedra. These bands have been assigned in a number of experimental and theoretical studies, but certain inconsistencies and points of disagreement persist among the results of different studies. These are discussed to allow a consistent band assignment. Infra-red reflection experiments have been carried out by Servoin and Piriou (1973) and Iishi (1978) for forsterite, by Stidham *et al.* (1976) for tephroite, and by Hohler and Funck (1969, 1973) for forsterite, tephroite and monticellite. Only Servoin and Piriou, and Iishi, carried out complete analyses of the reflection data by classical dispersion theory. Stidham *et al.* (1976) did not recalculate their reflection spectra to obtain mode frequencies, but used powder transmission data to estimate transverse optic (TO) mode frequencies, and the variation of reflection with angle of incidence (see below) to obtain approximate longitudinal (LO) frequencies. Hohler and Funck (1973) apparently took their mode frequencies at the maxima in their reflection spectra, hence their tabulated frequencies in Tables III–VI are overestimated and incorrect, although their reflection data are of good quality. Iishi (1978) used his results for a normal mode analysis of forsterite, while Devarajan and Funck (1975) carried out a similar calculation using the infrared data of Servoin and Piriou (1973), and the Raman spectra of Hohler and Funck (1973). There is some disagreement among the above experimental studies related to the presence of extra modes in some spectra and relative band intensities, which may be simply reconciled.

When a weak mode is present near a stronger band of slightly higher frequency, the oscillator strength of the weak mode may be overestimated to the detriment of the stronger band, without noticeable effect on the fit of experimental and calculated spectra. If the data of Servoin and Piriou (1973) and Iishi (1978) for the pair of B_{2u} modes at 875 and 838 cm^{-1} are compared, the oscillator strength of the weaker mode seems better reproduced by Iishi ($\Delta\varepsilon = 0.08$). A similar transfer of intensity has occurred for the B_{3u} modes observed at 978 and 952 cm^{-1}. However, the 952 cm^{-1} frequency may be an artifact in the B_{3u} spectrum, as discussed below.

Comparison of all the experimental reflection spectra above reveals a number of modes not predicted by theory in some spectra, which are not always observed, and which vary in relative intensity between authors. For anisotropic crystals, the infrared reflection spectrum becomes a non-linear combination of modes of different symmetries when the incident beam does not coincide with a principal crystallographic axis (*e.g.*, Alain and Piriou, 1971). For a given experimental configuration, one can show that the response function Im $(1/\varepsilon)$ (resonance function for LO modes in a spectrum of pure symmetry) gives rise to maxima at the frequencies of LO modes involved in the quasi-spectra above, independent of their symmetry. It follows that the reflection spectra of these quasi-modes show minima near the frequencies of each LO mode in the combination spectrum, which become more marked with increasing LO mode intensity (with a greater peak surface in Im $(1/\varepsilon)$). This was used by Stidham *et al.* (1976) in an attempt to determine their LO mode frequencies for tephroite. For measurements in normal incidence, the beam aperture and small orientation errors may lead to the appearance of artifacts, due to strong LO modes of one symmetry leaking into spectra of another nominal symmetry. This may be observed in the reflection spectra for the olivines, and accounts for the extra modes at 957 cm^{-1} (B_{3u}: LO of B_{2u} at 962.5), 962 cm^{-1} (B_{1u}: LO of B_{2u} at 962.5) and 1030 cm^{-1} (B_{2u}: LO of B_{3u} at 1081), which may be eliminated.

The 957 cm^{-1} frequency was taken into account by Iishi (1978) as a TO mode in his normal mode calculation. This may explain the incompatibility of the experimental oscillator strength at $\Delta\varepsilon = 0.12$ and the small calculated TO–LO splitting (less than 1 cm^{-1}, independent of the

model used), and the general poor fit of observed and calculated ν_3-derived frequencies. On the other hand, the weak B_{3u} mode only observed by Servoin and Piriou (1973) at 877 cm^{-1} (TO–LO splitting of 1 cm^{-1}) was not considered by Iishi although it is probably the second ν_3 component in B_{3u} symmetry. This is consistent with the calculation of Devarajan and Funck (1975), who ignored the 957 cm^{-1} frequency and used the B_{3u} mode at 877 cm^{-1}, to obtain a better fit of the Davydov splitting. The above discussion also applies to the B_{3u} spectrum of Stidham *et al.* (1976) for tephroite, where the true, weak B_{3u} mode was not observed, and the apparent B_{3u} frequency at 914 cm^{-1} corresponds to leakage of a strong LO component from the B_{2u} spectrum.

Raman results. For forsterite, Griffith (1969) assigned the 826 cm^{-1} Raman band to ν_1, and that near 860 cm^{-1} to ν_3, based on their relative intensities. However, in his Table 2, both modes appear as "strong" bands. The relative intensities of these bands vary with sample orientation, as seen from the single crystal studies of Servoin and Piriou (1973) and Iishi (1978). The Mn_2SiO_4 sample of Stidham *et al.* (1976) showed a similar relative intensity variation for the two most intense A_g modes. The relative intensities of these bands cannot then be simply used to distinguish their ν_1- or ν_3-derived character.

Several authors (*e.g.*, Tarte, 1963; Toropov *et al.*, 1963) have tabulated the variation of ν_1 and ν_3 frequencies of orthosilicates from infrared measurements against mean cation radius. It was shown by White (1975) that such plots did not show any simple systematics. (However, see later in this discussion.) For this study it was thought that following the Raman spectra through the olivine series Mg_2SiO_4–$CaMgSiO_4$–γ-Ca_2SiO_4 might show systematic differences between the two bands in question, giving support to some attribution. As seen from Figures 1 and 7 and Table 2, the two bands of interest appear to vary in a similar way along the series, allowing no distinction between them.

The results of vibrational calculations for olivines do not allow the ν_1- and ν_3-derived A_g modes to be distinguished either. In their vibrational analysis for forsterite, Devarajan and Funck (1975) assigned the A_g 822 cm^{-1} band to ν_1, as for the B_{1g} (B_{2g} in the Devarajan–Funck coordinate system) at 835 cm^{-1}. The original fit was poor, even for internal modes of SiO_4, and a new fit was made using the correct (C_s) symmetry for the SiO_4 units, with "corresponding" force constants. The ν_3 band at 960 cm^{-1} shared the same set of force constants as their ν_1 band at 835 cm^{-1} while a different set appeared for their ν_3 band at 854 cm^{-1}. This apparent reversal of roles was observed for other ν_1 and ν_3 force constant sets. On closer examination of the main force constant sets, each one appeared based only on ν_3-type motions, involving stretching of three out of four Si–O bonds, along with an angular O–Si–O interaction constant. No set corresponding to ν_1-type vibrations was found, which might have been expected, even with a nontetrahedral SiO_4 unit. These authors noted some difficulty with their force constant refinement. The calculation of Iishi (1978) also chose ν_1 as his 826 cm^{-1} band, and the associated B_{1g} at 839 cm^{-1}. This calculation did not give good agreement with experiment for high frequency Raman-active modes, and none of the displacement vectors reflect pure ν_3-type motions.

Finally, Pâques-Ledent and Tarte (1973) carried out ^{28}Si–^{30}Si isotopic substitution experiments on Mg_2SiO_4, and obtained Raman spectra in an attempt to definitely assign the 826 and 855 cm^{-1} bands. They cited Griffith (1969) as having chosen 855 cm^{-1} as ν_1 (he in fact chose 826 cm^{-1}) for its intensity. The ν_1-derived band should involve much less movement of Si than ν_3-derived vibrations, even for distorted tetrahedra, and hence such an isotopic experiment should discern the ν_1- and ν_3-derived modes. Pâques-Ledent and Tarte concluded that, since all bands showed an isotope effect, the two bands in question must have mixed ν_1–ν_3 character. We generally agree with this conclusion, but note also that the 855 cm^{-1} band shifted less than the others, suggesting more ν_1-character for this mode. This is also consistent with the earlier comparison of $CaMgSiO_4$ glass and crystal spectra, which suggested ν_1-character for the 852 cm^{-1} mode of monticellite due to its coincidence with the glass band assigned to ν_1. It is of interest that Pâques-Ledent and Tarte found the expected isotopic shifts for their infrared experiment, suggesting that ν_1–ν_3 coupling is less important for IR-active bands than for Raman-active vibrations in the olivines. This was also suggested by the comparison of symmetry and normal coordinates for infrared vibrations considered above.

Vibrational mode coupling

From the isotopic exchange studies, it is obvious that there exists considerable coupling between Raman-active ν_1–ν_3-derived vibrations of similar frequency. This coupling may be better understood by consideration of a simple system of two coupled harmonic oscillators, characterized by their coordinates x_1 and x_2 and a coupling constant β^2. The equations of motion are:

$$\ddot{x}_1 + \omega_1^2 x_1 - \beta^2 x_2 = 0$$

$$\ddot{x}_2 + \omega_2^2 x_2 - \beta^2 x_1 = 0$$

where ω_1 and ω_2 are the resonant frequencies in the absence of coupling (referred to below as the "pure" frequencies). Solution of this system of simultaneous equations leads to the two eigenfrequencies Ω_+ and Ω_-, where

$$\Omega_\pm^2 = \frac{\omega_1^2 + \omega_2^2}{2} \pm \left[\left(\frac{\omega_1^2 + \omega_2^2}{2}\right)^2 + \beta^4\right]^{1/2} \quad (1)$$

The normal coordinates $Q_\pm$ corresponding to the coupled frequencies $\Omega_\pm$ are given by:

$$Q_+ = a_1x_1 - a_2x_2 \quad (2a)$$

$$Q_- = a_2x_1 + a_1x_2 \quad (2b)$$

where

$$a_1 = \frac{\beta^2}{\beta^2 + \Omega_+^2 - \omega_1^2} \quad (3a)$$

and

$$a_2 = \frac{\beta^2}{\beta^2 - \Omega_-^2 + \omega_1^2} \quad (3b)$$

if one normalizes $a_1 + a_2 = 1$. From these expressions, the two oscillators vibrate in opposition for the higher frequency mode Ω_+, and in phase for Ω_- at lower frequency. In the following discussion, we neglect damping terms for simplicity, which should not greatly affect the eigenfrequencies, nor the relation between a_1 and a_2.

If for a given coupling, the pure frequencies ω_1 and ω_2 vary with some physical parameter X, it remains possible to calculate the coupled frequencies Ω_+ and Ω_-. For instance, this is the case for structures with coupled modes of which one shows soft mode behavior (*e.g.*, Alain and Piriou, 1977). In the case of the olivines, a number of studies have considered the variation of IR and Raman bands with composition (Tarte, 1963; Toropov *et al.*, 1963; Duke and Stephens, 1964; Burns and Huggins, 1972; White, 1975; this work, Figure 7). It is evident that both ν_1- and ν_3-derived modes show a general decrease in frequency from forsterite to γ-Ca_2SiO_4, while the site-group splitting of the ν_3-derived vibrations also appears to decrease. The structural factors responsible for these changes may be embodied in some parameter X, with which the pure, uncoupled frequencies ω_i are assumed to vary linearly. The pure (uncoupled) frequencies for the three A_g modes derived from ν_1 and ν_3 motions are assumed to be: $\omega_1 = 858$, $\omega_2 = 848$ and $\omega_3 = 993$ cm^{-1}. These frequencies are assumed to vary as $\omega_1(\text{cm}^{-1}) = 858 - 24X$; $\omega_2(\text{cm}^{-1}) = 848 - 11.5X$; $\omega_3(\text{cm}^{-1}) = 993 - 43.5X$, as shown in Figure 8. Modes ω_1 and ω_2 are strongly coupled, and Figure 8 shows the variation of the coupled frequencies Ω_+ and Ω_- with X for a coupling constant $\beta = 160$ cm^{-1}. Also shown in Figure 8 are the observed high-frequency A_g modes for forsterite, monticellite, tephroite and γ-Ca_2SiO_4 from Table 2, placed so that the highest frequency mode observed lies on the line calculated for ω_3. The calculated coupled frequencies for Ω_+ and Ω_- show reasonable agreement with the experimental frequencies for the remaining two ν_1- and ν_3-derived modes. We note, however, that this coupling diagram is only intended to be schematic. We have no way of relating the parameter X to structural effects within the olivines, and the variations of ω_1, ω_2 and ω_3 are not necessarily linear functions of X. Finally, the "pure" frequencies ω_1, ω_2 and ω_3 were only estimated for this discussion, while the coupling parameter β need not necessarily be constant. The diagram does indicate that a simple coupling scheme may be used to describe the ν_1- and ν_3-derived Raman-active modes in the olivine series.

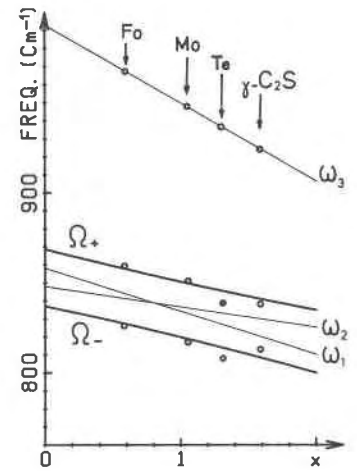

Fig. 8. Schematic coupling diagram for high-frequency modes of the olivine structure, applicable to A_g and B_{1g} species. This may be compared with the observed frequency variation in Figure 7. The parameters X, ω_1, ω_2, ω_3, Ω_+ and Ω_- are explained in the text.

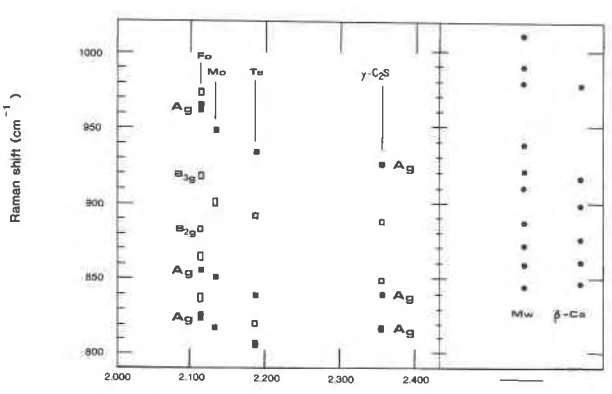

Fig. 7. Variation with ⟨M(1)–O⟩ of Raman frequencies from Table 2. The merwinite and larnite points are not plotted *vs.* ⟨M(1)–O⟩, but are shown for comparison with the olivine values. The size of the points for Raman frequencies represents the range of observed values from the studies quoted in Table 2. A_g modes are shown by full rectangles: other symmetries by boxes.

Figure 7 shows the observed Raman frequencies for forsterite, monticellite, tephroite and γ-Ca_2SiO_4 plotted against the average M(1)–O bond length, as for the structural parameters discussed earlier. This may be compared with the schematic coupling scheme in Figure 8. It is beyond the scope of this article to discuss the coupling in detail, since both pure ν_1- and ν_3-derived band frequencies and the coupling parameter must vary in a complex way with composition, being dependent on a variety of structural and dynamic factors.

The proposed coupling scheme implies a cross-over of modes of ν_1- and ν_3-type which may be justified as follows. The calcic olivine γ-Ca_2SiO_4 was shown earlier to have the most regular SiO_4 tetrahedral units, hence the least ν_1-ν_3 coupling, while the degree of coupling should increase through tephroite and monticellite to forsterite. The ν_1-derived mode of γ-Ca_2SiO_4 was found near 815 cm^{-1} in the powder infrared studies of Tarte (1963) and Oehler and Günthard (1969). This suggests the attribution of the strong A_g Raman mode near 815 cm^{-1} (Boyer in publicity for Jobin-Yvon MOLE: see notes to Table 2; this study, Figure 1) to a ν_1-type vibration in a system with little ν_1–ν_3 coupling. On the other hand, the isotopic studies on forsterite (Pâques-Ledent and Tarte, 1973) showed that the A_g Raman band at 855 cm^{-1} had more ν_1 character than the strong A_g mode at lower frequency, although both are strongly coupled. These observations agree with a coupling scheme with cross-over of bands of pure ν_1 and ν_3 character, as drawn in Figure 8.

When X is small, the normal coordinates Q_+ and Q_- (Equation 2) are dominated by x_1 and x_2 respectively. This is reversed for large X, with a continuous transfer of character, as described by the linear equations. The Raman intensity of the ν_1- and ν_3-derived A_g modes is related to their proportion of ν_1 character. This may be seen from Figure 1, where the highest-frequency A_g mode has little ν_1-character, and is much less intense than the other two A_g modes. These two intense A_g modes undergo a transfer of Raman intensity in the series forsterite–monticellite–γ-Ca_2SiO_4 (Fig. 1), which is in agreement with the coupling scheme of Figure 8, where χ_1 and χ_2 correspond to the symmetry coordinates relative to ν_1 and ν_3 shown in Figure 6. We consider that γ-Ca_2SiO_4 is least affected by ν_1–ν_3 coupling, with its strong A_g band of lower frequency being predominantly ν_1 in character. As the coupling increases towards forsterite, the higher frequency strong A_g band takes on more ν_1 character, transferring ν_3 character to the lowest frequency A_g. The olivines monticellite and tephroite lie in a region of strong ν_1–ν_3 coupling, where neither band has well-defined character. The two strong A_g bands for monticellite are nearly equal in intensity (Fig. 1), suggesting that monticellite lies near the crossover point of a_1 and a_2 (Fig. 9) where both modes have equal ν_1- and ν_3-character. This implies that the coincidence of the 854 cm^{-1} mode in monticellite glass and crystal discussed earlier is fortuitous. The above model will also hold for the B_{1g} modes associated with the A_g vibrations by the Davydov splitting.

The coupling scheme does not appear so simple for the infra-red active vibrations. The ν_1-derived IR band for γ-Ca_2SiO_4 appears weak in the powder spectra of Tarte (1963) and Oehler and Günthard (1969), consistent with little ν_1–ν_3 coupling as above, and increases in intensity for monticellite, tephroite and fayalite (Tarte, 1963; Burns and Huggins, 1972) as expected. However, this band then decreases in intensity between fayalite and forsterite, suggesting a decrease in ν_1–ν_3 coupling. The IR-active bands do not show a frequency cross-over and change of character as do the Raman spectra, suggesting a more complex coupling scheme for the olivine infrared spectra. However, it was noted earlier that vibrational mode coupling cannot be important in these spectra, from a consideration of band intensities.

Relationship between orthosilicate high-frequency bands and structure

This final section considers a number of general correlations between the structure and high-frequency vibrational spectra of olivines and related orthosilicates. It was noted earlier that the frequencies of ν_1- and ν_3-derived modes in olivine decreased with increasing M(1) cation size, which may be correlated with the general increase in average Si–O bond length from forsterite to γ-Ca_2SiO_4 (Figure 5a). This may be contrasted with comparable glass spectra, where the ν_1 frequency was found to vary little with composition. The ν_1-derived modes for the olivine structure γ-Ca_2SiO_4 are found near 815 cm^{-1} compared with 860 cm^{-1} for ν_1 of SiO_4 in calcium silicate glasses. However, a strong band is found in the Raman spectrum of larnite near 860 cm^{-1} (β-Ca_2SiO_4; Fig. 2) which may be assigned to a ν_1-derived A_g mode in this non-olivine structure. We suggest that formation of γ-Ca_2SiO_4 with its high degree of polyhedral edge-sharing results in an expansion of the SiO_4 tetrahedra to accomodate the large Ca^{2+} on both M(1) and M(2) sites, and is responsible for the lowered Si–O stretching frequencies. The larnite structure has much less tetrahedral–octahedral edge-sharing, and allows the SiO_4 tetrahedra to relax to approximately their free-ion geometry, with a central stretch frequency similar to that in the glass. The available structure refinement for β-Ca_2SiO_4 is not precise enough to confirm this for the tetrahedral Si–O distances.

Merwinite ($Ca_3MgSi_2O_8$) has no shared polyhedral edges, and its average Si–O distances are less than those for the olivines (Fig. 5a). This is manifested in its Raman

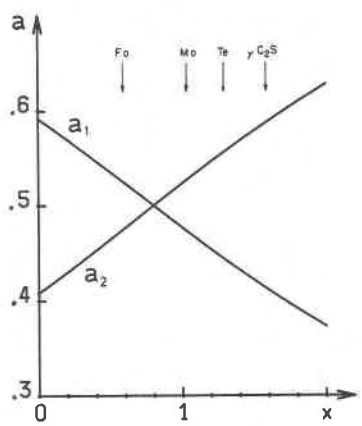

Fig. 9. Variation of the coefficients a_1 and a_2, which determine the relative character of ω_1 and ω_2, with X for the same conditions as Figure 8.

spectrum (Fig. 2b; Table 2), where the silicate stretch vibrations appear at higher frequencies than for the olivines. Similarily, tricalcium silicate (Ca_3SiO_5) contains SiO_4 units linked only by their corners to calcium–oxygen polyhedra, with mean Si–O distances smaller than in the olivines (Golovastikov *et al.*, 1976). Its principal, and presumably ν_1-derived, Raman bands occur at 845 and 855 cm^{-1} (Conjeaud and Boyer, 1980), near that of ν_1 in the glass.

Not only do the absolute frequencies of Si–O stretch vibrations decrease along the olivine series from forsterite to γ-Ca_2SiO_4, but also the site-group splitting of the ν_3-derived modes (Fig. 7). As the SiO_4 unit is distorted from tetrahedral symmetry, this splitting is expected to increase, although the ν_1–ν_3 coupling discussed above may complicate this behavior. The observed decrease in ν_3 splitting may be related to the converging trends of tetrahedral distances and angles as M(1) becomes larger (Fig. 5), giving a more symmetric SiO_4 unit as γ-Ca_2SiO_4 is approached. Jeanloz (1980) has compared the infrared spectra of a number of silicate olivines and spinels. In the cubic spinel structure, the SiO_4 unit has tetrahedral symmetry (Brown, 1980), and no splitting of ν_3-type vibrations would be expected. The spinel spectra showed a single major high-frequency band which Jeanloz (1980) assigned to ν_3 motions of SiO_4, with weaker bands attributed to tetrahedral-octahedral site vibrational interactions. The reduction in ν_3 splitting with increase in SiO_4 symmetry is consistent with the above discussion for the olivine series.

Conclusion

This study began as a simple comparison of $CaMgSiO_4$ glass and its corresponding crystal, but since grew into a survey of the vibrational spectroscopic and structural literature on the olivines. We have attempted to identify a consistent set of high-frequency Raman and infrared modes for olivine, with suggested assignments to vibrational types. We suggest that vibrational mode coupling between ν_1- and ν_3-derived vibrations is important for the Raman-active A_g and related B_{1g} modes, but less so for infrared-active modes. This should be taken into account in future lattice dynamical calculations, along with the correct band assignments. Frequency shifts of ν_1- and ν_3-derived modes, and the degree of ν_3 splitting, may be correlated with systematic changes in the geometry of the SiO_4 unit, although these may be complicated by ν_1–ν_3 coupling. Finally, it seems that the original point of this study—the coincidence of the Raman band near 850 cm^{-1} in $CaMgSiO_4$ crystal and glass—is entirely fortuitous. We suggest that the two intense A_g modes in the monticellite spectrum have almost equal ν_1 and ν_3 character, while that for $CaMgSiO_4$ glass is pure ν_1.

Acknowledgments

The authors gratefully acknowledge support from the French CNRS and the PIRPSEV program, and from the National Science Foundation (grants EAR-78-09954-02 and INT-79-26523). We thank G. M. Biggar for providing the $CaMgSiO_4$ gel, J. P. Coutures for help with the solar furnace preparations, and J. Etchepare for the use of his Raman laboratory for the merwinite spectrum. We are grateful to J. Clark, J. Bradley and A. Yates for their assistance with sample analyses, carried out in the Chemistry Department at A.S.U.. A. Navrotsky and J. Holloway read and commented on original versions of this manuscript, which was typed by V. Rehder, N. Dagon and M. Palitz. Finally, we thank R. Jeanloz, G. Rossman and an anonymous reviewer for their helpful and constructive criticisms.

References

Aden, G. D. and Buseck, P. R. (1979). Rapid quantitative analysis of individual particles by energy-dispersive spectrometry. In D. E. Newbury, Ed., Microbeam Analysis, p. 254–258. San Francisco Press Inc.

Alain, P. and Piriou, B. (1971). Etude infrarouge et Raman des vibrations de réseau de L'Aluminate de Néodyme. Physica Status Solidi, 43, 669–680.

Alain, P. and Piriou, B. (1977). Transition de phase à haute temperature dans les aluminates de terre rare. Journal de Physique, 12, C7, 389–394.

Basso, R., Dal Negro, A., Della Giustia, A. and Rossi, G. (1979). Fe/Mg distribution in the olivine of ultramafic nodules from Assab (Ethiopia). Neues Jahrbuch für Mineralogie, Monatshefte, 5, 197–202.

Biggar, G. M. and O'Hara, M. J. (1969). Monticellite and forsterite crystalline solutions. Journal of the American Ceramic Society, 52, 249–252.

Birle, J. D., Gibbs, G. V., Moore, P. B. and Smith, J. V. (1968). Crystal structures of natural olivines. American Mineralogist, 53, 807–824.

Bretheau-Raynal, F., Dalbiez, J. P., Drifford, M. and Blanzat, B. (1979). Raman spectroscopic study of thortveitite structure silicates. Journal of Raman Spectroscopy, 8, 39–42.

Brown, G. E. (1970). The crystal chemistry of the olivines. Ph.D. Thesis, Virginia Polytechnic Institute and State University, Blacksburg, Virginia (not seen: referenced data appears in Brown (1980)).

Brown, G. E. (1980). Olivines and silicate spinels. In P. H. Ribbe, Ed., Orthosilicates, p. 275–381. Reviews in Mineralogy, Volume 5, Mineralogical Society of America.

Brown, G. E. and Prewitt, C. T. (1973). High temperature crystal chemistry of hortonolite. American Mineralogist, 58, 577–587.

Burns, R. G. and Huggins, F. E. (1972). Cation determinative curves for Mg–Fe–Mn olivines from vibrational spectra. American Mineralogist, 57, 967–985.

Conjeaud, M. and Boyer, H. (1980). Some possibilities of Raman microprobe in cement chemistry. Cement and Concrete Research, 10, 61–70.

Coons, W. E. (1978). Cobalt as an analogue for iron in high temperature experiments on basaltic compositions. Ph.D. Thesis, Arizona State University, Tempe, Arizona.

Coutures, J. P., Berjoan, R., Benezech, G. and Granier, B. (1978). Utilisation des fours solaires de laboratoire pour l'étude à haute temperature des propriétés physicochimiques des oxydes refractaires. Revue Internationale des Hautes Temperatures et Refractaires, 15, 103–114.

Cruikshank, D. W. J. (1964). Refinements of structures containing bonds between Si, P, S or Cl and O or N. X. β-Ca_2SiO_4.

Acta Crystallogaphica, 17, 685–686.
Czaya, R. (1971). Refinement of the structure of γ-Ca_2SiO_4. Acta Crystallogaphica, B27, 848–849.
Devarajan, V. and Funck, E. (1975). Normal coordinate analysis of the optically active vibrations (k=0) of crystalline magnesium orthosilicate Mg_2SiO_4 (forsterite). Journal of Chemical Physics, 62, 3406–3411.
Duke, D.A. and Stephens, G. D. (1964). Infrared investigation of the olivine group minerals. American Mineralogist, 49, 1388–1406.
Eysel, W. and Hahn, T. (1970). Polymorphism and solid solution of Ca_2GeO_4 and Ca_2SiO_4. Zeitschrift für Kristallographie, 131, 322–341.
Fateley, W. G., Dollish, F. R., McDevitt, N. T. and Bentley, F. F. (1972). Infrared and Raman selection rules for molecular and lattice vibrations: the correlation method. Wiley-Interscience, New York.
Finger, L. W. (1970). Fe/Mg ordering in olivines. Carnegie Institute of Washington Year Book, 69, 302–305.
Fortnum, D. and Edwards, J. O. (1956). The Raman spectrum and the structure of the aqueous silicate ion. Journal of Inorganic and Nuclear Chemistry, 2, 264–265.
Francis, C. A. and Ribbe, P. H. (1980). The forsterite–tephroite series: I. Crystal structure refinements. American Mineralogist, 65, 1263–1269.
Ghose, S. and Wan, C. (1974). Strong site preference of Co^{2+} in olivine, $Co_{1.10}Mg_{0.90}SiO_4$. Contributions to Mineralogy and Petrology, 47, 131–140.
Golovastikov, N. I., Matveeva, R. G. and Belov, N. V. (1976). Crystal structure of the tricalcium silicate $3CaO \cdot SiO_2 = C_3S$. Soviet Physics Crystallography, 20, 441–445.
Griffith, W. P. (1969). Raman spectroscopy of minerals. Nature, 224, 264–266.
Handke, M. and Ptaak, W. (1978). I.R. and Raman studies of the stabilization of β-Ca_2SiO_4. Ceramurgia International, 4, 75–78.
Hanke, K. (1965). Beiträge zu Kristallstrukturen vom Olivin-Typ. Beiträge zur Mineralogie und Petrographie, 11, 535–558.
Hazen, R. M. (1976). Effects of temperature and pressure on the crystal structure of forsterite. American Mineralogist, 61, 1280–1293.
Hazen, R. M. (1977). Effects of temperature and pressure on the crystal structure of ferromagnesian olivine. American Mineralogist, 62, 286–295.
Heinrich, K. F. J. (1972). A simple correction procedure for quantitative electron probe microanalysis. National Bureau of Standards Technical Note 719, U. S. Government Printing Offices.
Herzberg, G. (1945). Molecular Spectra and Molecular Structure. II. Infrared and Raman spectra of polyatomic molecules. Van Nostrand, New York.
Hohler, V. and Funck, E. (1969). Infrarot-Spektrum von Sinhalit und Olivin. Naturwissenschaften, 56, 459.
Hohler, V. and Funck, E. (1973). Vibrational spectra of crystals with olivine structure. I. Silicates. Zeitschrift für Naturforschung B, 28, 125–139.
Iishi, K. (1978). Lattice dynamics of forsterite. American Mineralogist, 63, 1198–1208.
Jeanloz, R. (1980). Infrared spectra of olivine polymorphs: α, β phase and spinel. Physics and Chemistry of Minerals, 5, 327–341.
Kashio, S. Iguchi, Y., Goto, T., Nishina, Y. and Fuwa, T. (1980). Raman spectroscopic study on the structure of silicate slag. Transactions of the Iron and Steel Institute of Japan, 20, 251–253.
Kusabiraki, K. and Shiraishi, Y. (1981). The infrared spectrum of vitreous fayalite. Journal of Non-Crystalline Solids, 44, 365–368.
Lager, G. A. and Meagher, E. P. (1978). High-temperature structural study of six olivines. American Mineralogist, 63, 365–377.
Lazarev, A. N. (1972). Vibrational spectra and structure of silicates. Consultants Bureau, New York.
Louisnathan, S. J. and Gibbs, G. V. (1972). Variation of Si–O distances in olivines, soda melilite and sodium metasilicate as predicted by semiempirical molecular orbital calculations. American Mineralogist, 57, 1643–1663.
McMillan, P. (1981). A structural study of aluminosilicate glasses by Raman spectroscopy. Ph.D. Dissertation, Arizona State University, Tempe, Arizona.
McMillan, P., Coutures, J. P. and Piriou, B. (1981). Diffusion Raman d'un verre de monticellite. Comptes Rendus de l'Academie de Sciences à Paris, Série II, 292, 195–198.
Midgley, C. M. (1952). The crystal structure of β dicalcium silicate. Acta Crystallographica, 5, 307–312.
Moore, P. B. and Araki, T. (1972). Atomic arrangement of merwinite, $Ca_3Mg(SiO_4)_2$, an unusual dense-packed structure of geophysical interest. American Mineralogist, 57, 1355–1374.
Morimoto, N., Tokonami, M., Watanabe, M. and Koto, K. (1974). Crystal structures of three polymorphs of Co_2SiO_4. American Mineralogist, 59, 475–485.
Mysen, B. O., Virgo, D. and Scarfe, C. M. (1980). Relations between the anionic structure and viscosity of silicate melts—a Raman spectroscopic study. American Mineralogist, 65, 690–710.
Nelson, B. N. and Exarhos, G. J. (1979). Vibrational spectroscopy of cation-site interactions in phosphate glasses. Journal of Chemical Physics, 71, 2739–2747.
Oehler, O. and Gunthard, Hs.H. (1969). Low-temperature infrared spectra between 1200 and 20 cm^{-1} and normal-coordinate analysis of silicates with olivine structure. Journal of Chemical Physics, 51, 4719–4727.
Onken, H. (1965). Verfeinerung der Kristallstruktur von Monticellite. Tschermaks Mineralogische und Petrographische Mitteilungen, 10, 34–44.
Pâques-Ledent, M.Th. and Tarte, P. (1973). Vibrational studies of olivine-type compounds—I. The i.r. and Raman spectra of the isotopic species of Mg_2SiO_4. Spectrochimica Acta, 29A, 1007–1016.
Rajamani, V., Brown, G. E. and Prewitt, C. T. (1975). Cation ordering in Ni–Mg olivine. American Mineralogist, 60, 292–299.
Servoin, J. L. and Piriou B. (1973). Infrared reflectivity and Raman scattering of Mg_2SiO_4 single crystal. Physica Status Solidi (b), 55, 677–686.
Smyth, J. R. (1975). High temperature crystal chemistry of fayalite. American Mineralogist, 60, 1092–1097.
Smyth, J. R. and Hazen, R. M. (1973). The crystal structures of forsterite and hortonolite at several temperatures up to 900°C. American Mineralogist, 58, 588–593.
Stidham, H. D., Bates, J. B. and Finch, C. B. (1976). Vibrational spectra of synthetic single crystal tephroite, Mn_2SiO_4. Journal of Physical Chemistry, 80, 1226–1234.
Tarte, P. (1963). Etude infra-rouge des orthosilicates et des

orthogermanates—II. Structures du type olivine et monticellite. Spectrochimica Acta, 19, 25–47.

Thomas, I. L. and Haukka, M. T. (1978). XRF determination of trace and major elements using a single-fused disc. Chemical Geology, 21, 39–50.

Toropov, N. A., Fedorov, N. F. and Shevyakov, A. M. (1963). Infrared absorption spectra of orthosilicates of some bivalent elements. Russian Journal of Inorganic Chemistry, 8(6), 697–699.

Virgo, A., Mysen, B. O. and Kushiro, I. (1980). Anionic constitution of silicate melts quenched at 1 atm from Raman spectroscopy: Implications for the structure of igneous melts. Science, 208, 1371–1373.

Warner, R. D. and Luth, W. C. (1973). Two-phase data for the join monticellite ($CaMgSiO_4$)–forsterite (Mg_2SiO_4): Experimental results and numerical analysis. American Mineralogist, 58, 1009–1015.

Wenk, H.-R. and Raymond, K. N. (1973). Four new structure refinements of olivine. Zeitschrift für Kristallographie, 137, 86–105.

White, W. B. (1975). Structural interpretations of lunar and terrestrial minerals of Raman spectroscopy. In C. Karr, Ed., Infrared and Raman spectroscopy of lunar and terrestrial materials, p. 325–358, Academic Press, New York.

Yamaguchi, G. and Suzuki, K. (1967). Structural analysis of merwinite. Journal of the Ceramic Association of Japan, 75, 220–229.

Manuscript received, April 2, 1982;
accepted for publication, September 20, 1982.